metals

MDPI

*Article*

# Effect of Boron-Free Niobium Addition on the Hot Tearing Susceptibility of the AlSi5Cu2Mg Alloy

**Martina Sýkorová *, Dana Bolibruchová and Marek Matejka**

Department of Technological Engineering, Faculty of Mechanical Engineering, University of Žilina, Univerzitná 8215/1, 010 26 Žilina, Slovakia; danka.bolibruchova@fstroj.uniza.sk (D.B.); marek.matejka@fstroj.uniza.sk (M.M.)
* Correspondence: martina.sykorova@fstroj.uniza.sk

**Abstract**

The AlSi5Cu2Mg alloy for cylinder-head castings is known for its pronounced susceptibility to hot tearing. This study examines how niobium additions affect the hot tearing susceptibility (HTS) of this alloy. Niobium was introduced via an AlNb10 master alloy in nominal amounts of 0.10, 0.15 and 0.20 wt.% (measured 0.049, 0.063 and 0.076 wt.%). HTS was evaluated quantitatively, by three variants of the hot tearing index (HTI) determined from tears on four arms of a five-arm restrained-contraction mould, and qualitatively, from the load recorded on the fifth, anchored arm. All niobium additions reduced the HTI values. The lowest values were obtained for the nominal 0.15 wt.% addition ($HTI_1$ = 0.18, $HTI_2$ = 0.60 and $HTI_3$ = 0.17 compared with 0.93, 2.35 and 1.91 for the reference alloy). In the qualitative evaluation, this was the only alloy in which no anchored arm separated. In contrast, two anchored arms of the 0.20 wt.% Nb alloy separated immediately and a third transferred less than 120 N. This occurred despite the finest dendritic structure (secondary dendrite arm spacing 16.58 versus 25.76 μm). Niobium can therefore reduce the HTS of the AlSi5Cu2Mg alloy, with the most favourable effect at a nominal addition of 0.15 wt.%.

**Keywords:** AlSi5Cu2Mg alloy; niobium; Al-Nb master alloy; hot tearing susceptibility; hot tearing index; secondary dendrite arm spacing

## 1. Introduction

Hypoeutectic Al-Si-Cu-Mg casting alloys are widely used for thermally and mechanically loaded automotive components, above all for cylinder heads. They combine low density and good castability with precipitation strengthening by Cu- and Mg-bearing phases, which provides the required strength at elevated temperatures [1,2]. The AlSi5Cu2Mg alloy studied here was developed for cylinder-head castings. Its chemical composition is tightly specified and limits the Ti content to a maximum of 0.03 wt.%. This limit practically excludes the standard Al-Ti-B grain refiners, because their effective additions would exceed the permitted Ti content. Consequently, the alloy cannot be grain-refined by conventional means. It is also known for its high susceptibility to hot tearing [3,4].

Hot tears form in the last stage of solidification. At this stage, the dendrites already form a coherent network that can transmit stress, but the grains are still separated by thin films of residual liquid. If the thermal contraction of the network is restrained by the mould or by a colder part of the casting, the strain concentrates in these films. When the interdendritic liquid can no longer compensate for the strain and the shrinkage, the films open and a tear forms [5–7]. The key alloy-related factors are the width of the vulnerable temperature range, the permeability of the mushy zone and the amount and distribution of

Check for updates

Academic Editor: Shusen Wu

Received: 30 September 2026
Revised: 5 November 2026
Accepted: 14 November 2026
Published: 17 November 2026

**Copyright:** © 2026 by the authors. Licensee MDPI, Basel, Switzerland. This article is an open access article distributed under the terms and conditions of the Creative Commons Attribution (CC BY) license.

the last-solidifying eutectic. The mould design and the mould and pouring temperatures are the main process-related factors [7,8].

Among the alloy-related factors, the Fe-rich intermetallic phases are of particular importance. Iron is the most common impurity in Al-Si casting alloys, especially when recycled material is used. At the usual cooling rates, it precipitates mainly as the β-$Al_5FeSi$ phase in the form of thin, brittle platelets [9]. These platelets form in the interdendritic regions before or together with the Al-Si eutectic. Besides reducing ductility, they block the interdendritic channels through which the residual melt compensates for the solidification shrinkage. For this reason, iron is associated with increased porosity and other feeding-related defects [10]. The morphology of the Fe-rich phases directly affects feeding in the stage of solidification in which hot tears form.

Grain refinement is one of the most effective metallurgical means of reducing hot tearing. Fine equiaxed grains shift the dendrite coherency point to a higher solid fraction and distribute the strain over more grain boundaries. They also keep the interdendritic channels permeable for longer, so that the residual melt can heal incipient tears [11–13]. In an Al-Zn-Mg-Cu alloy, a smaller grain size lowered the contraction stress and increased the number of feeding channels available for the healing of tears [14]. In Al-Si alloys, however, Ti-based refiners lose efficiency as the Si content increases. This effect, known as Si poisoning, occurs because titanium reacts with silicon to form Ti-Si-containing phases that no longer act as nucleants [15]. In the AlSi5Cu2Mg alloy, Ti additions beyond the specified limit reduced the hot tearing index [4]. Because of the strict Ti limit and the lower efficiency of Ti in Si-containing melts, new inoculants outside the Al-Ti-B system are being developed, with attention focused on other transition metals.

Among these alternatives, niobium is particularly promising. Niobium belongs, together with V and Ta, to the group 5 transition metals. Similarly to the group 4 metals Ti, Zr and Hf, these elements form $Al_3M$ trialuminides and peritectic systems with aluminium, and they have a low solubility and a very low diffusivity in solid aluminium [16]. The peritectic $Al_3Nb$ phase is isostructural with $Al_3Ti$, which makes it a potential nucleant for α-Al [17]. Nowak et al. [17] and Bolzoni et al. [18] showed that Nb-B inoculation refines the grain size of binary and commercial Al-Si alloys. Unlike Ti-based nuclei, Nb-based substrates remain effective over a wide range of Si contents and solidification conditions [19]. They promote equiaxed grains even under directional solidification [20]. Niobium also affects the Fe-rich phases. In recycled Al-Si alloys with 1 wt.% Fe, Nb-B additions made the β-Fe precipitates much smaller and more spheroidal [21]. In our previous study on the AlSi5Cu2Mg alloy with the same nominal Nb additions, a boron-free Nb addition reduced the mean size of the β-$Al_5FeSi$ platelets from 22.6 to 11.6 µm. It also promoted more compact Fe-rich phases [22].

Niobium can therefore influence both the α-Al dendrites and the Fe-rich intermetallics, the two microstructural features that control feeding at the end of solidification. To the authors' knowledge, however, its effect on the hot tearing susceptibility of Al-Si-Cu-Mg alloys has not yet been studied, and this applies in particular to Nb added without boron, which is of interest for alloys with a restricted Ti content.

The aim of this study is to determine whether a boron-free Nb addition can reduce the hot tearing susceptibility of the AlSi5Cu2Mg alloy and to identify the most suitable amount of the addition. Nominal Nb additions of 0.10, 0.15 and 0.20 wt.% were introduced through an AlNb10 master alloy. The hot tearing susceptibility was evaluated quantitatively, by three variants of the hot tearing index, and qualitatively, from the load and temperature recorded on the anchored arm. From a practical point of view, an effective addition that respects the Ti limit could lower the hot tearing susceptibility of this alloy in cylinder-head production, where conventional Al-Ti-B refiners cannot be used. In contrast to our previous

studies, which addressed the effect of Zr and Ti on the hot tearing of this alloy [3,4] and the effect of Nb on its Fe-rich phases [22], the present work evaluates the effect of Nb on its hot tearing susceptibility.

## 2. Materials and Methods

### *2.1. Experimental Material and Melt Preparation*

The hypoeutectic AlSi5Cu2Mg alloy used for the production of cylinder-head castings was supplied by Nemak Slovakia s.r.o. (Žiar nad Hronom, Slovakia). Four variants were prepared: the reference alloy without niobium and alloys with nominal additions of 0.10, 0.15 and 0.20 wt.% Nb. The base alloy was melted in a LAC T15 electric resistance furnace (LAC, Židlochovice, Czech Republic) with an open atmosphere. The melt temperature was kept at 750 ± 5 °C. It was measured with an AHLBORN THERM 2420-1L thermometer (AHLBORN, Prague, Czech Republic) with a type K (NiCr-Ni) thermocouple (5TC series, OMEGA Engineering, Norwalk, CT, USA). To ensure complete dissolution, the AlNb10 master alloy (Holtec, Prague, Czech Republic) for each Nb variant was melted separately in an electric induction furnace (Indutherm, Walzbachtal, Germany) and the molten master alloy was transferred into the AlSi5Cu2Mg melt. The melt was not intentionally degassed. Consistent degassing with an inert gas using a rotary degasser is not possible for the small melt volume used in laboratory experiments; in such cases, degassing tablets are used instead. These tablets are based on chloride and fluoride salts and react violently and exothermically with the aluminium melt. In a small melt volume, their residues may remain in the melt as exogenous inclusions [23]. The same procedure was applied in our previous study on the effect of Ti on the hot tearing of this alloy [4]. The reference alloy without Nb was cast from the same melt under identical conditions. The hydrogen content of all alloys can therefore be considered comparable.

The chemical composition of the experimental alloys, determined by a VANTA X-ray fluorescence spectrometer (Evident, Waltham, MA, USA), is given in Table 1. The Ti content of all alloys (0.027–0.028 wt.%) remained below the specified limit of 0.03 wt.%. The measured Nb contents (0.049, 0.063 and 0.076 wt.%) correspond to a recovery of 49, 42 and 38% of the nominal additions. The recovery decreased with increasing addition. This is probably related mainly to the settling of the dense $Al_3Nb$ particles in the crucible, which has been observed for Nb-based master alloys in unstirred Al-Si melts [24]. The designations of the alloys used in this work correspond to the nominal additions. As the measured Nb contents increase in the same order as the nominal additions, the ranking of the alloys and the observed trends are not affected by this choice.

**Table 1.** Chemical composition of the experimental alloys [wt.%].

| Alloy | Si | Cu | Mg | Mn | Fe | Ti | Sr | Nb | Al |
|---|---|---|---|---|---|---|---|---|---|
| Reference | 6.45 | 2.54 | 0.15 | 0.015 | 0.23 | 0.028 | 0.004 | – | bal. |
| Nb 0.10 | 6.52 | 2.40 | 0.18 | 0.012 | 0.23 | 0.028 | 0.004 | 0.049 | bal. |
| Nb 0.15 | 6.58 | 2.46 | 0.19 | 0.014 | 0.23 | 0.027 | 0.005 | 0.063 | bal. |
| Nb 0.20 | 6.82 | 2.34 | 0.19 | 0.012 | 0.22 | 0.028 | 0.006 | 0.076 | bal. |

### *2.2. Hot Tearing Test*

The hot tearing susceptibility was evaluated using the restrained-contraction device shown in Figure 1, which is identical to the device used in previous studies [4]. The mould cavity consists of a central sprue and five arms of different length. Four of them (64.5, 104.5, 124.5 and 184.5 mm) terminate in spherical ends that restrain the contraction of the solidifying arm. The fifth, longest arm serves as the measuring arm. An anchoring bolt is cast into its end and connected to an S9M force transducer (HBM, Darmstadt, Germany),

which records the tensile load caused by the restrained contraction. The temperature of the melt was measured with a K-type thermocouple placed in the mould cavity next to the inlet (position 7 in Figure 1b). As the thermocouple is not located in the measuring arm, the recorded temperatures characterise the solidification stage of the casting only approximately. The signals were acquired with a NI USB-9162 Hi-Speed USB carrier with a C Series input module (National Instruments, Austin, TX, USA) and recorded continuously in LabVIEW (version 25.3, National Instruments). The metal mould was coated with graphite and preheated to 150 ± 10 °C. Its temperature was checked with a VOLTCRAFT IR 900-30S infrared thermometer (VOLTCRAFT, Hirschau, Germany). The pouring temperature was 750 °C, and five test castings were produced from each alloy. The pouring and mould temperatures were the same for all alloys and all castings. The hot tearing susceptibility was evaluated quantitatively from the tears on the four arms with spherical ends (Section 2.3) and qualitatively from the load record of the measuring arm (Section 2.4).

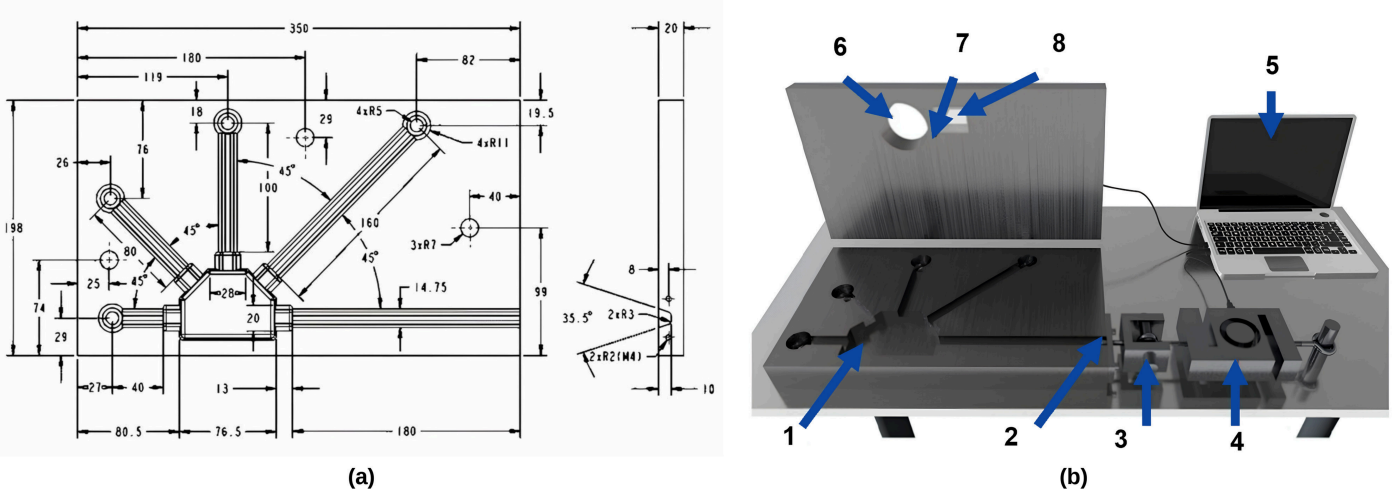



**Figure 1.** Hot tearing test: (**a**) scheme of the mould (dimensions in mm); (**b**) measuring device: 1—mould, 2—anchoring bolt, 3—clamping mechanism, 4—force transducer, 5—data acquisition and processing, 6—inlet, 7—thermocouple; 8—refractory glass. Adapted from [4].

### *2.3. Quantitative Evaluation Method*

The quantitative evaluation was based on the tears observed on the four arms with spherical ends. Three variants of the hot tearing index (HTI) were calculated. The first variant, $HTI_1$, follows Wu [25] and depends on the number of tears (NT), their severity expressed by the weighting factor (WF) and the number of evaluated arms (NA):

$$HTI_1 = \frac{NT \cdot \sum WF}{NA}, \quad (1)$$

The second variant, $HTI_2$, is based on the approach of Akhyar et al. [26], summarised by Song et al. [27]. It also takes into account the arm length, expressed by the arm length coefficient (ALC), and the tear position, expressed by the tear position coefficient (TPC):

$$HTI_2 = \sum WF \cdot TPC \cdot ALC, \quad (2)$$

The weighting factor WF is assigned according to the severity of the tear (Figure 2), and the values of ALC and TPC are listed in Table 2. The third variant, $HTI_3$, combines both approaches [4]:

$$HTI_3 = \frac{NT \cdot \sum (WF \cdot ALC \cdot TPC)}{NA}, \quad (3)$$




**Figure 2.** Tear severity categories and the corresponding weighting factors WF. Adapted from [4].

**Table 2.** Arm length coefficient (ALC) and tear position coefficient (TPC) [4].

| Arm | ALC | Tear Position | TPC |
|---|---|---|---|
| Arm 1 (64.5 mm) | 1 | Lower part of the arm | 1 |
| Arm 2 (104.5 mm) | 2 | Upper part of the arm | 2 |
| Arm 3 (124.5 mm) | 3 | Middle part of the arm | 3 |
| Arm 4 (184.5 mm) | 4 | – | – |

The index values were averaged over the five castings of each alloy, reported as the mean ± standard deviation and classified into five hot tearing susceptibility (HTS) categories according to Table 3 [4]. In the text, HTI without a subscript refers to all three indices.

**Table 3.** Hot tearing susceptibility (HTS) categories. Adapted from [4].

| HTI Value | <0.5 | 0.5–1.25 | 1.25–2.25 | 2.25–3.5 | >3.5 |
|---|---|---|---|---|---|
| HTS | Minimal | Low | Moderate | High | Very high |

### *2.4. Qualitative Evaluation Method*

During solidification, the load on the anchoring bolt and the temperature were recorded at a sampling frequency of 4 Hz. The load rate $(dF/dt)$ was calculated as the time derivative of the load, smoothed with a Savitzky–Golay filter (6 s window) to suppress the signal noise. The time was counted from the moment of pouring, identified by the steep rise of the temperature signal.

Three types of arm behaviour were distinguished: no hot tear, hot tear and immediate arm separation. An arm without a hot tear shows a continuous increase in the load. An immediate separation is indicated by the absence of any load transfer. A hot tear was identified when the load build-up was delayed or markedly reduced and a tear was found on the arm. Hot tear initiation was taken as the first load pickup that was followed by a stagnation or a markedly reduced rate of load increase. The end of tear propagation was taken as the renewed continuous increase in the load. A threshold of 10 N was used to identify the hot tear initiation and a threshold of 30 N to identify the end of tear propagation, so that both events were distinguished from the signal noise. The thresholds were set above the noise of the load signal and are small compared with the maximum loads (up to 1137 N). The classification of the arms is based on the course of the load record and on the visual inspection and does not depend on the threshold values; different thresholds would only slightly shift the determined times and temperatures of the events. The events were determined from the load record and not from the load rate. The load rate responds to the change in slope already when the load is still within the signal noise, and the smoothing window further shifts its rise to slightly earlier times. The onset of $\mathrm{d}F/\mathrm{d}t$ therefore precedes the moment at which the load exceeds the threshold, although both reflect the same event.

For each test, the temperature, time, maximum load and maximum load rate within the first 150 s after pouring were determined. All measuring arms were inspected visually.

### *2.5. Metallography*

Metallographic samples were prepared by wet grinding and polishing and etched with 0.5% HF. To reveal the Fe-rich phases, selected samples were etched in a solution of 20 mL $H_2SO_4$ and 100 mL $H_2O$. The microstructure and the tear profiles were examined with a Keyence VHX-7000 digital microscope (Keyence, Osaka, Japan). The Nb 0.20 alloy, i.e., the alloy with the highest Nb content, was additionally examined after deep etching, which removes the α-Al matrix and exposes the intermetallic particles, using a TESCAN LMU II scanning electron microscope (TESCAN, Brno, Czech Republic) with a Bruker Quantax EDX analyzer (Bruker, Berlin, Germany), including elemental mapping. The secondary dendrite arm spacing (SDAS) was determined by the linear intercept method as

$$\mathrm{SDAS} = \frac{\mathrm{L}}{\mathrm{n}-1}, \tag{4}$$

where SDAS is the secondary dendrite arm spacing (µm) and L (µm) is the length of the line drawn along a dendrite trunk, perpendicular to the secondary arms, from the first to the last of n secondary dendrite arms. The measurements were carried out on light micrographs using the measuring tool of the VHX-7000 software. The SDAS was measured on samples taken from the castings of the hot tearing test. The reported values are the mean and standard deviation of five measurements per alloy.

## 3. Results and Discussion

### *3.1. Quantitative Evaluation*

The values of the three hot tearing indices are shown in Figure 3. The reference alloy reached $HTI_1 = 0.93 \pm 0.49$, $HTI_2 = 2.35 \pm 0.96$ and $HTI_3 = 1.91 \pm 1.24$, corresponding to low, high and moderate susceptibility, respectively. The different categories result from the multiplication by ALC and TPC in $HTI_2$ and $HTI_3$; all three indices nevertheless rank the alloys in the same way, with the highest value for the reference alloy and the lowest for the Nb 0.15 alloy.

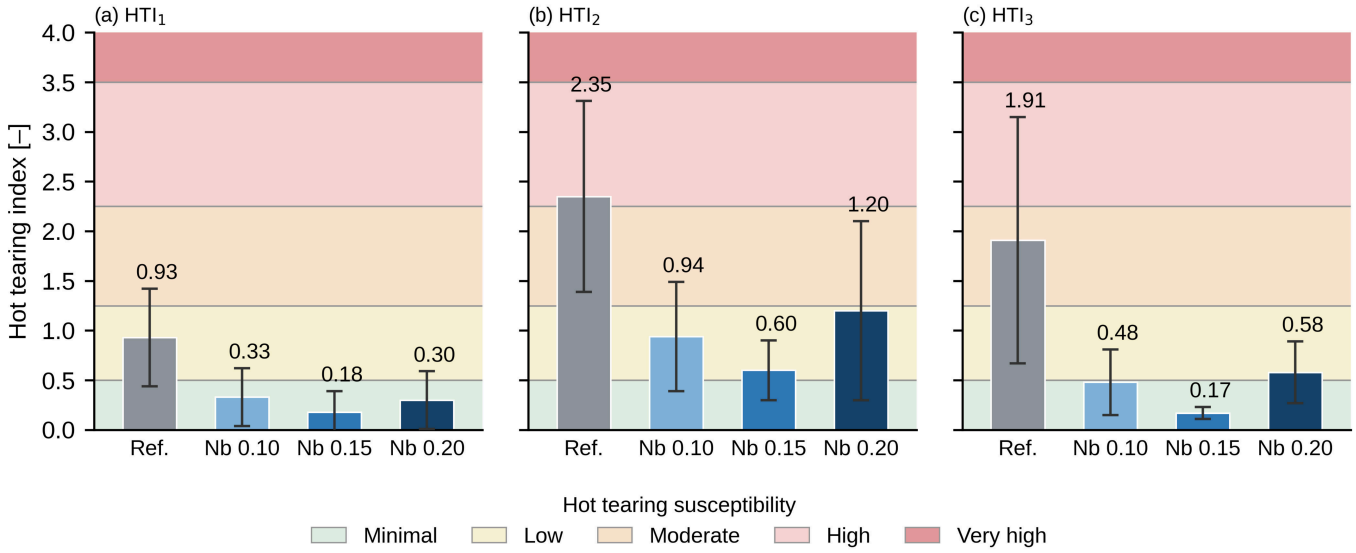



**Figure 3.** Hot tearing indices (**a**) $HTI_1$, (**b**) $HTI_2$ and (**c**) $HTI_3$ of the reference alloy and the alloys with Nb addition; the shaded zones correspond to the hot tearing susceptibility categories according to Table 3; the error bars show the standard deviation of five castings.

All three Nb additions reduced every index compared with the reference alloy. The addition of 0.10 wt.% Nb lowered the indices to $HTI_1 = 0.33 \pm 0.29$, $HTI_2 = 0.94 \pm 0.55$ and $HTI_3 = 0.48 \pm 0.33$, which corresponds to reductions of 65, 60 and 75%. The alloy moved to the minimal ($HTI_1$, $HTI_3$) and low ($HTI_2$) susceptibility categories. The lowest values were obtained for the Nb 0.15 alloy, with $HTI_1 = 0.18 \pm 0.21$, $HTI_2 = 0.60 \pm 0.30$ and $HTI_3 = 0.17 \pm 0.06$, representing reductions of 81, 74 and 91%. For the Nb 0.20 alloy, all three indices increased again ($HTI_1 = 0.30 \pm 0.29$, $HTI_2 = 1.20 \pm 0.90$, $HTI_3 = 0.58 \pm 0.31$; reductions of 68, 49 and 70%), and $HTI_3$ moved from the minimal to the low category. Nevertheless, the values remained below those of the reference alloy. The indices show a non-monotonic dependence with a minimum at the nominal addition of 0.15 wt.% Nb (0.063 wt.% measured). Given the scatter of the results, this minimum should be regarded as a trend. The error bars of the three Nb alloys overlap, so the differences between them cannot be distinguished from the scatter of the individual castings. However, the Nb 0.15 alloy was the only alloy whose range of mean ± standard deviation did not overlap with that of the reference alloy for any of the three indices. Its identification as the most favourable addition is further supported by the independent evaluation with the anchored measuring arm (Section 3.2).

### *3.2. Qualitative Evaluation*

The results of the qualitative evaluation are given in Tables 4–7, and typical records together with the corresponding castings are shown in Figures 4–7. In the reference alloy (Table 4), the measuring arm separated immediately in tests 3 and 4. The remaining three arms showed a continuous increase in the load without a hot tear and reached maximum loads of 940–1030 N and maximum load rates of 34.0–53.7 $N \cdot s^{-1}$ (Figure 4a,c). In the separated arms, no load was transferred during the whole test (Figure 4b).

**Table 4.** Qualitative evaluation of the reference alloy.

| Test No. | Tear Formation | | | | End of Propagation |
|---|---|---|---|---|---|
| | Temperature [°C] | Time [s] | Load [N] | Load Rate [$N \cdot s^{-1}$] | |
| 1 | no hot tear | – | max. 940 | max. 53.4 | no hot tear |
| 2 | no hot tear | – | max. 1030 | max. 53.7 | no hot tear |
| 3 | immediate separation | – | – | – | immediate separation |
| 4 | immediate separation | – | – | – | immediate separation |
| 5 | no hot tear | – | max. 948 | max. 34.0 | no hot tear |

**Table 5.** Qualitative evaluation of the Nb 0.10 alloy.

| Test No. | Tear Formation | | | | End of Propagation |
|---|---|---|---|---|---|
| | Temperature [°C] | Time [s] | Load [N] | Load Rate [$N \cdot s^{-1}$] | |
| 1 | immediate separation | – | – | – | immediate separation |
| 2 | 548 | 11.2 | max. 563 | max. 19.1 | reduced load build-up |
| 3 | no hot tear | – | max. 1029 | max. 37.3 | no hot tear |
| 4 | no hot tear | – | max. 861 | max. 35.8 | no hot tear |
| 5 | immediate separation | – | – | – | immediate separation |

In the Nb 0.10 alloy (Table 5), the measuring arm separated immediately in tests 1 and 5, which is the same frequency as in the reference alloy. In test 2, a hot tear formed at 548 °C at the onset of loading, about 11 s after pouring. It did not interrupt the load build-up, but it reduced the maximum load rate to 19.1 $N \cdot s^{-1}$ and the maximum load to 563 N (Figure 5a). The tear is clearly visible on the arm (Figure 5c). Tests 3 and 4 showed

a continuous increase in the load up to 1029 and 861 N. The arm of test 3 remained intact. On the arm of test 4, a small tear was found that did not affect the load record.

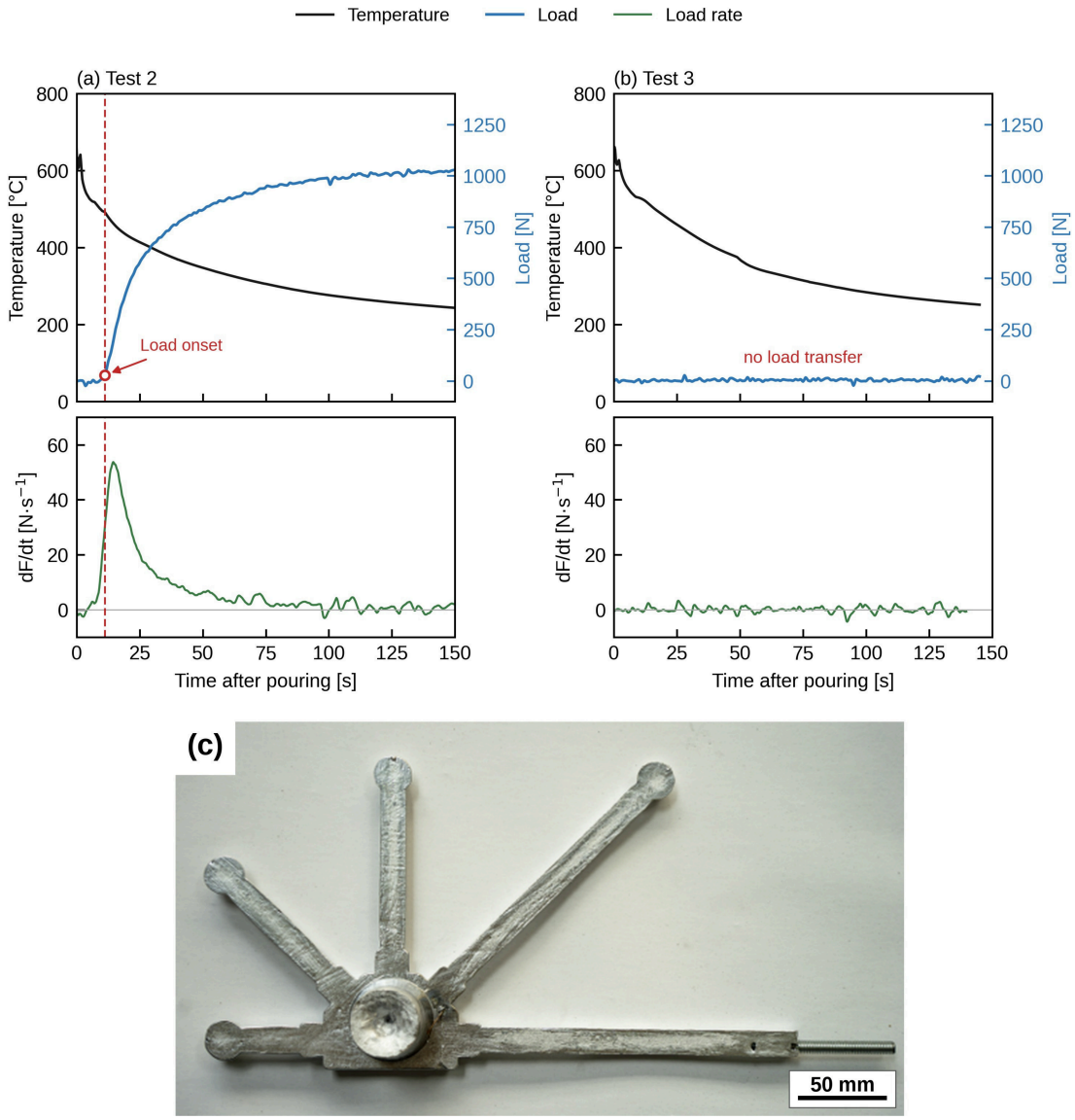



**Figure 4.** Load, temperature and load rate records of the reference alloy: (**a**) test 2, no hot tear; (**b**) test 3, immediate separation; (**c**) casting from test 2. Dashed lines mark the load onset.

**Table 6.** Qualitative evaluation of the Nb 0.15 alloy.

| Test No. | Tear Formation | | | | End of Propagation |
|---|---|---|---|---|---|
| | Temperature [°C] | Time [s] | Load [N] | Load Rate [N·s$^{-1}$] | |
| 1 | no hot tear | – | max. 848 | max. 53.4 | no hot tear |
| 2 | no hot tear | – | max. 1137 | max. 55.0 | no hot tear |
| 3 | no hot tear | – | max. 951 | max. 50.2 | no hot tear |
| 4 | 558 | 10.2 | max. 517 | max. 26.1 | increase in load (525 °C, 16.8 s) |
| 5 | no hot tear | – | max. 1042 | max. 40.8 | no hot tear |

The Nb 0.15 alloy (Table 6) was the only variant in which no arm separated. Four of the five arms showed a continuous increase in the load, with maximum loads of 848–1137 N and maximum load rates of 40.8–55.0 N·s$^{-1}$ (Figure 6a). Small tears were nevertheless

found on the arms of tests 1 and 5. They were confined to the surface at the transition between the arm and the bolt head and did not affect the load. In test 4, the load picked up at 558 °C but then stopped increasing. A continuous increase started again only at 525 °C, 6.6 s later (Figure 6b). The maximum load of this arm reached only 517 N, about half of the value of the intact arms. The tear across the measuring arm of this casting is visible in Figure 6c.

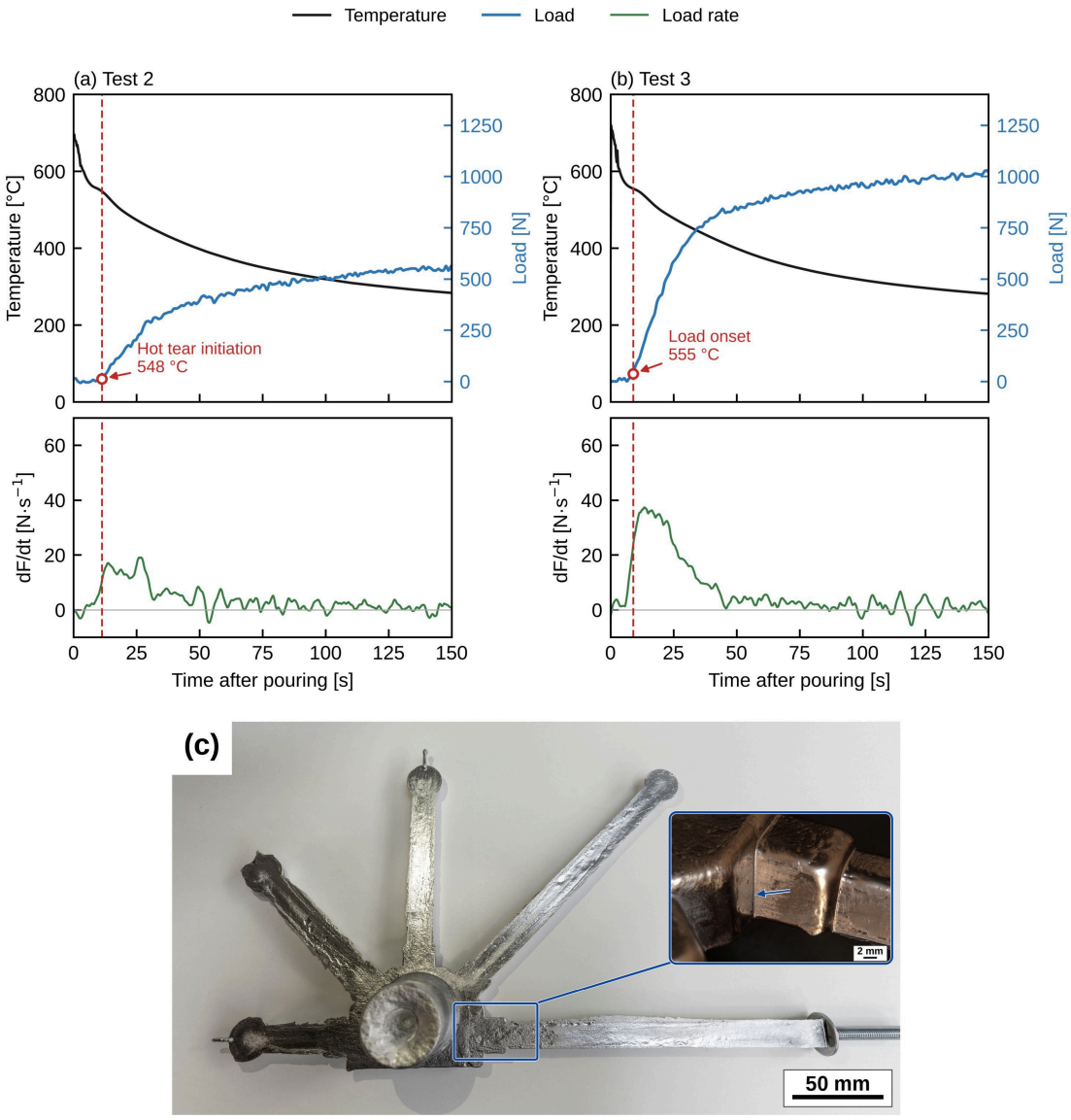



**Figure 5.** Load, temperature and load rate records of the Nb 0.10 alloy: (**a**) test 2, hot tear; (**b**) test 3, no hot tear; (**c**) casting from test 2 with an enlarged detail of the tear (arrow). Dashed lines mark the hot tear initiation or the load onset.

The Nb 0.20 alloy (Table 7) performed worst. The measuring arm separated immediately in tests 1 and 4 (Figure 7a,c). In test 3, a hot tear formed at 548 °C. The load then increased only slowly, without a distinct renewed onset, to a maximum of 114 N (Figure 7b). Test 5 also showed a hot tear with a delayed increase in load, but its initiation could not be determined unambiguously from the record (Table 7). Only the arm of test 2 built up load continuously, and even this arm contained a small tear.

**Table 7.** Qualitative evaluation of the Nb 0.20 alloy.

| Test No. | Tear Formation | | | | End of Propagation |
|---|---|---|---|---|---|
| | Temperature [°C] | Time [s] | Load [N] | Load Rate [N·s$^{-1}$] | |
| 1 | immediate separation | – | – | – | immediate separation |
| 2 | no hot tear | – | max. 790 | max. 37.2 | no hot tear |
| 3 | 548 | 10.8 | max. 114 | max. 6.7 | no distinct increase in load |
| 4 | immediate separation | – | – | – | immediate separation |
| 5 | indeterminate | – | max. 470 | max. 13.7 | increase in load |

Indeterminate: a hot tear was found on the arm and the load build-up was delayed, but the tear initiation could not be determined unambiguously from the load record.

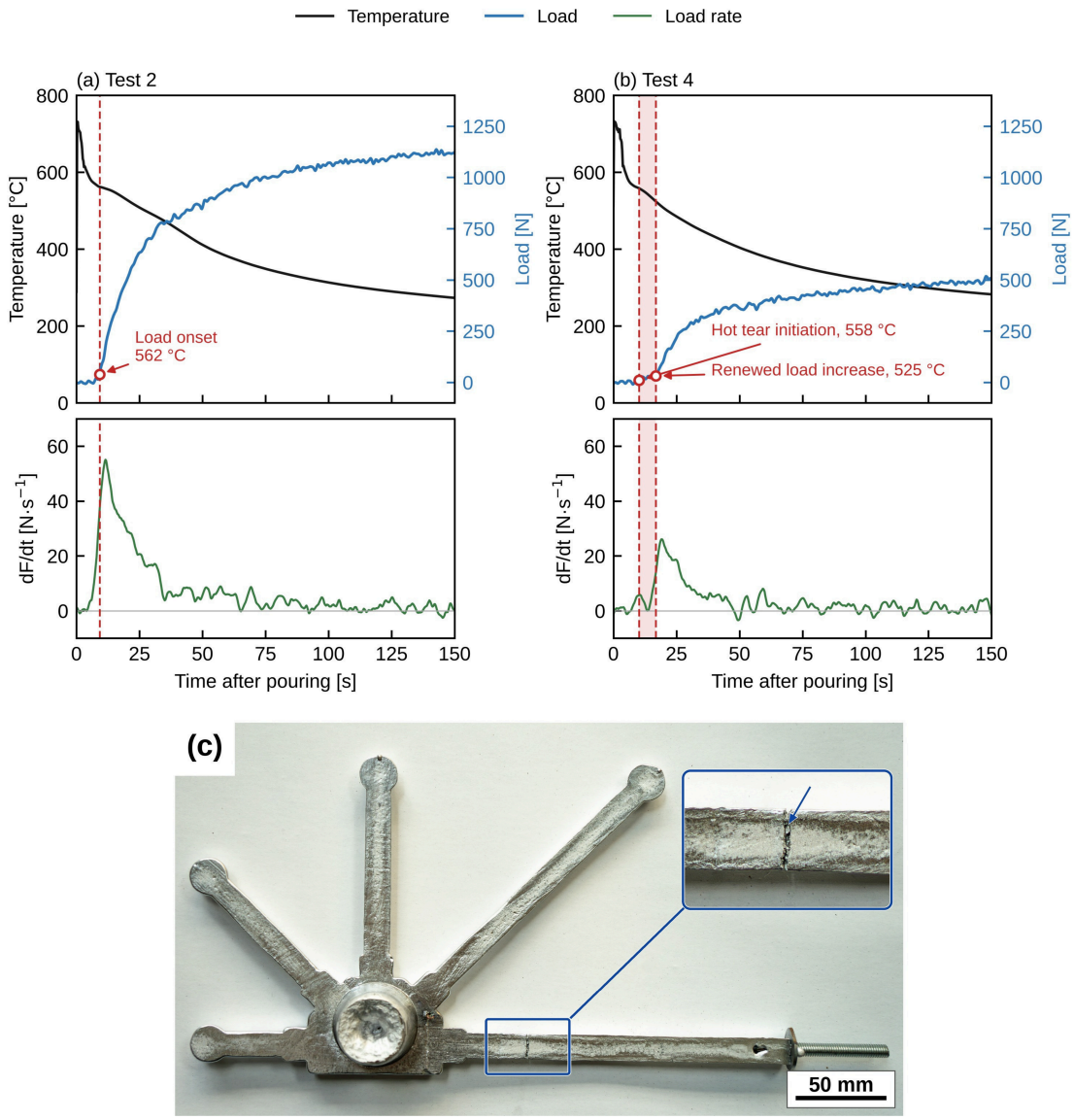



**Figure 6.** Load, temperature and load rate records of the Nb 0.15 alloy: (**a**) test 2, no hot tear; (**b**) test 4, hot tear; (**c**) casting from test 4 with an enlarged detail of the tear (arrow). Dashed lines mark the hot tear initiation or the load onset; the shaded area marks the interval between hot tear initiation and the renewed increase in load.

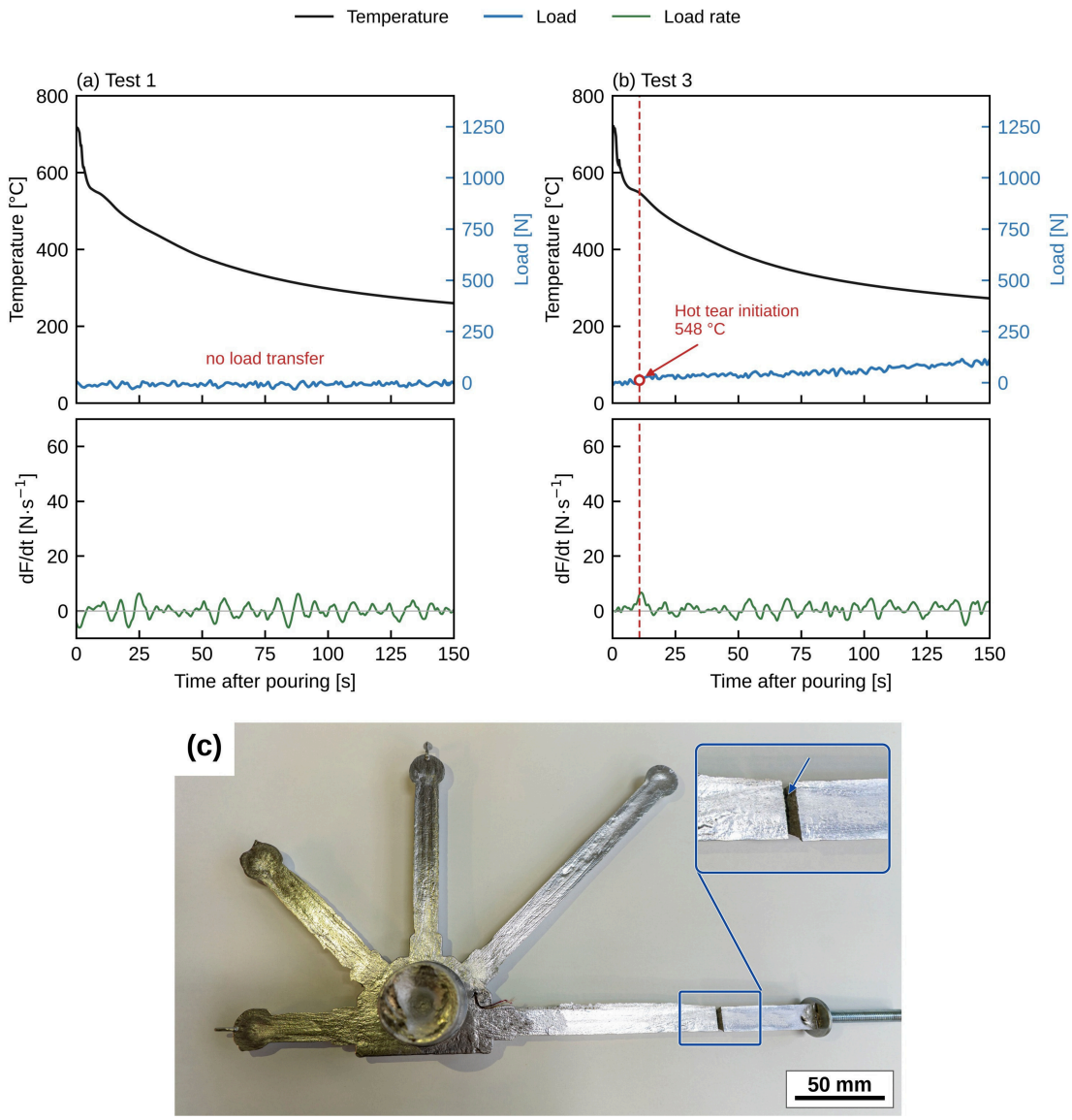



**Figure 7.** Load, temperature and load rate records of the Nb 0.20 alloy: (**a**) test 1, immediate separation; (**b**) test 3, hot tear; (**c**) casting from test 1 with an enlarged detail of the separated arm (arrow). Dashed lines mark the hot tear initiation.

The results are summarised in Table 8. Only the Nb 0.15 alloy improved the behaviour of the anchored arm compared with the reference alloy. No arm separated, and four of its five arms built up the load continuously to 848–1137 N. The Nb 0.10 alloy behaved similarly to the reference alloy, and in the Nb 0.20 alloy, two arms separated immediately and no arm remained free of tears.

**Table 8.** Summary of the qualitative evaluation of the anchored measuring arm (number of tests out of five).

| Alloy | No Hot Tear in the Load Record | Hot Tear in the Record | Immediate Arm Separation | Arms Without Any Visible Tear |
|---|---|---|---|---|
| Reference | 3 | 0 | 2 | 3 |
| Nb 0.10 | 2 | 1 | 2 | 1 |
| Nb 0.15 | 4 | 1 | 0 | 2 |
| Nb 0.20 | 1 | 2 | 2 | 0 |

Small surface tears found by visual inspection that did not affect the load record are not counted as hot tears in the record.

In all arms without a hot tear in the record, the load onset occurred 7–12.5 s after pouring, in the final stage of solidification. The temperature recorded at that moment was 555–577 °C for the Nb alloys and 492–522 °C for the reference alloy. This indicates that a continuous, load-bearing dendritic network capable of transmitting the contraction stress forms in the arm only in this stage. The hot tears identified in the records initiated at 548–558 °C, at the lower end of the range recorded for the Nb alloys or slightly below it. This is the moment when the arm started to be loaded and the interdendritic liquid could no longer compensate for the contraction. As the thermocouple is located in the mould cavity next to the inlet (Figure 1b) and not in the measuring arm, these temperatures characterise the solidification stage of the casting only approximately and do not represent the local temperature of the arm. For the same reason, and because the load onset occurred within the same time interval in all alloys, the higher onset temperatures recorded for the Nb alloys are not interpreted as an effect of niobium.

Both evaluations agree in identifying the nominal 0.15 wt.% addition as the most favourable. For the Nb 0.10 and Nb 0.20 alloys, however, they differ. Both alloys have HTI values below the reference alloy, but their anchored arms behaved like the reference alloy (Nb 0.10) or even worse (Nb 0.20). The two evaluations reflect different levels of restraint. The divergence can be quantified by the mean maximum load of the anchored arms, with the separated arms counted as zero: compared with 584 N for the reference alloy, it was 491, 899 and 275 N for the Nb 0.10, Nb 0.15 and Nb 0.20 alloys, whereas $HTI_3$ decreased from 1.91 to 0.48, 0.17 and 0.58, respectively. The HTI is determined from four arms that are restrained only by their spherical ends. The measuring arm, in contrast, is the longest arm of the casting and is rigidly anchored, so it accumulates the largest contraction strain. A small Nb addition is enough to suppress tearing under moderate restraint, but only the nominal 0.15 wt.% addition also withstood the severe restraint of the anchored arm.

### *3.3. Microstructure and Secondary Dendrite Arm Spacing*

The as-cast microstructure of all alloys (Figure 8) consisted of primary α-Al dendrites, the Al-Si eutectic and Cu- and Fe-rich intermetallic phases located in the interdendritic regions. The eutectic Si did not exhibit the coarse plate-like morphology, which appears as needles in the metallographic section and is typical of the unmodified as-cast state. Instead, it precipitated as fine, rounded to fibrous particles. This indicates that the alloy was supplied by the producer in a pre-modified state, most likely with strontium (Table 1). Although the Sr content (0.004–0.006 wt.%) is at the lower end of the range usually used for modification, the fine eutectic Si indicates a modified state. With increasing Nb addition, the α-Al dendrites became finer and more uniformly distributed, and the Fe-rich phases appeared shorter and more compact than in the reference alloy. No Nb-containing particles were identified by light microscopy in the alloys with Nb. SEM-EDS mapping of the deep-etched Nb 0.20 alloy (Figure 9) did not reveal any Nb-bearing phases either. Silicon was concentrated in the eutectic and copper and iron in the intermetallic phases, whereas the Nb signal was distributed uniformly at the background level, without any local enrichment (Figure 9f). As the measured Nb contents (0.049–0.076 wt.%) are below the typical detection limit of EDS, niobium is most likely dissolved in the α-Al matrix. Undissolved master-alloy particles, which could act as nucleation sites or as inclusions, were therefore not found in the castings; the niobium that did not enter the melt most likely settled in the crucible (Section 2.1).

The SDAS values are shown in Figure 10. The SDAS decreased monotonically from 25.76 µm for the reference alloy to 20.06, 18.36 and 16.58 µm for the Nb 0.10, Nb 0.15 and Nb 0.20 alloys (by 22, 29 and 36%). SDAS is controlled primarily by the local solidification

time, and all castings were produced at the same mould and pouring temperatures. The decrease indicates that Nb refines the dendritic structure.

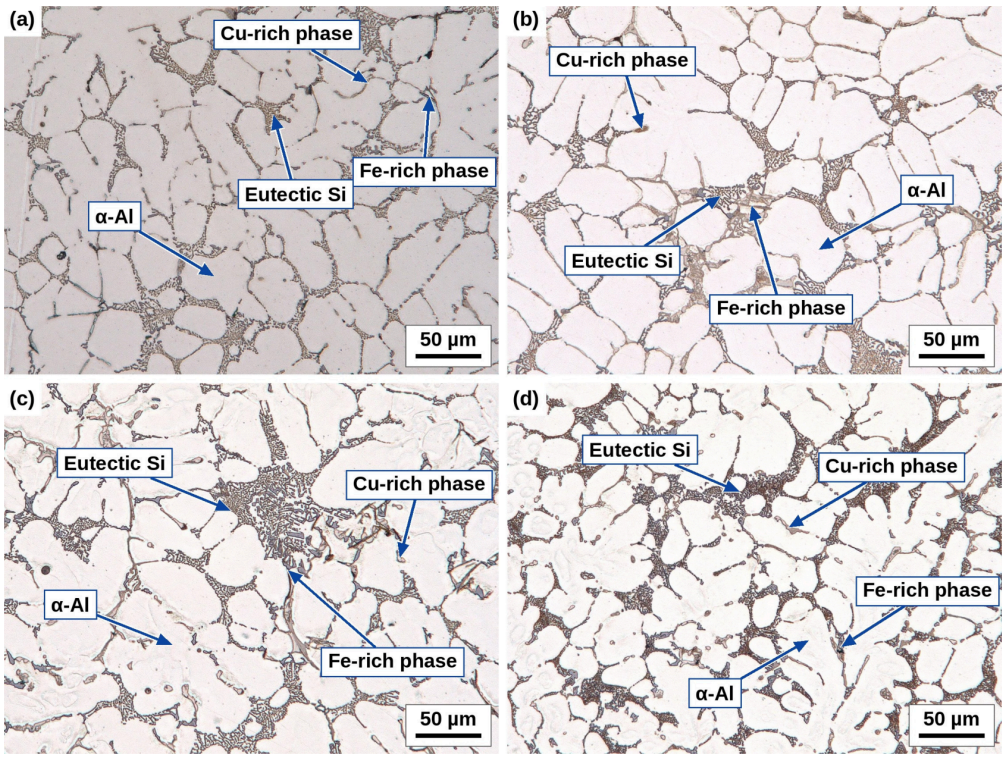



**Figure 8.** As-cast microstructure: (**a**) reference alloy; (**b**) Nb 0.10; (**c**) Nb 0.15; (**d**) Nb 0.20.

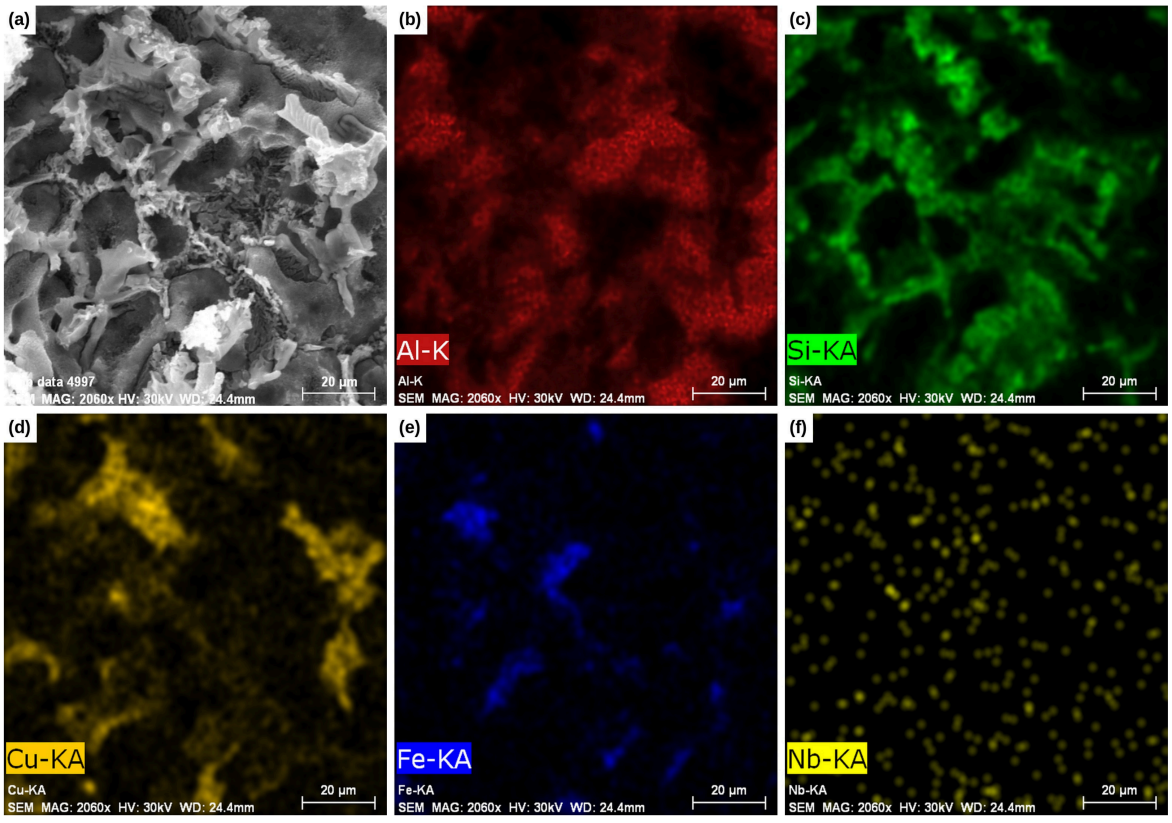



**Figure 9.** SEM-EDS analysis of the deep-etched Nb 0.20 alloy: (**a**) SEM image; (**b**–**f**) elemental maps of Al, Si, Cu, Fe and Nb.

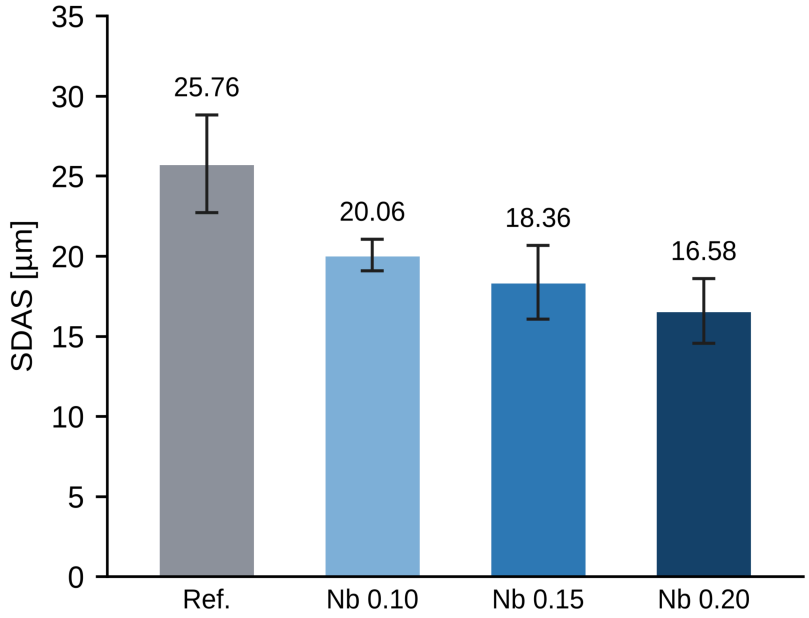



**Figure 10.** Secondary dendrite arm spacing (SDAS) of the experimental alloys; the error bars show the standard deviation of five measurements.

Tear profiles in the measuring arm of the Nb 0.20 alloy are shown in Figure 11; the black areas are the tear openings filled with the mounting resin. The macroscopic section of the measuring arm (Figure 11a,b) shows the course of the tear and its side branches. The tears run along the interdendritic regions, and their walls are formed by free, rounded dendrite arms that protrude into the opening without any sign of fracture (Figure 11c,d). This indicates that the dendrite arms grew freely into the residual liquid and that the opening formed by the separation of liquid films rather than by the fracture of solid material. Microshrinkage pores occur directly at the tear edge (Figure 11c). They mark regions where the interdendritic liquid was no longer fed; under the contraction strain, such regions may have acted as sites from which the tear opened. Side branches of the main tear and interdendritic cavities follow the eutectic regions between the dendrites (Figure 11b,d,e). A fragment of the dendritic network was separated from the tear wall, and a eutectic-rich region lines the opening next to it (Figure 11e). This region suggests that residual eutectic liquid penetrated into the opening but was not sufficient to fill it. These features are typical of hot tears [5,7]. After etching for Fe-rich phases, the Fe-rich intermetallic particles are visible in the interdendritic regions between the α-Al dendrites, together with the Al-Si eutectic (Figure 11f).

### *3.4. Effect of Niobium on Hot Tearing*

The hot tearing behaviour of the Nb alloys can be related to two microstructural changes caused by niobium. Both concern the feeding of the mushy zone in the vulnerable stage of solidification. The first is the refinement of the dendritic structure, documented here by the decrease in SDAS (Figure 10). A finer dendritic structure divides the residual liquid into a larger number of interdendritic channels and distributes the contraction strain over more interdendritic regions. Incipient tears can then be healed, as long as the flow of liquid through these channels is sufficient [11,14]. The growth restriction factor Q of the dissolved niobium, estimated from its slope $m(k-1) = 6.6$ K/wt.% [28], is only about 0.3–0.5 K, compared with about 50 K for the alloy as a whole, which is dominated by Si. Growth restriction by dissolved Nb alone is therefore unlikely to explain the decrease in SDAS. The mechanism by which Nb refines the dendritic structure remains to be clarified; the presence of fine Nb-containing particles below the resolution of the methods used

cannot be excluded. The second is the change of the Fe-rich phases. In the AlSi5Cu2Mg alloy with the same nominal Nb additions, the β-$Al_5FeSi$ platelets became shorter with increasing Nb content, from 22.6 µm without Nb to 19.1, 14.9 and 11.6 µm for 0.10, 0.15 and 0.20 wt.% Nb, and the Fe-rich phases became more compact [22] (Table 9). These values were determined on samples of the same Nb-containing melts cast into a metal mould [22]. As the Fe and Mn contents of the Nb alloys were practically the same (0.22–0.23 wt.% Fe, 0.012–0.014 wt.% Mn), the progressive shortening of the platelets with increasing Nb content can be attributed to niobium. Because the cooling conditions in the metal mould differ from those in the hot tearing mould, these data indicate the trend rather than the exact platelet size in the present castings; the Fe-rich phases in the hot tearing castings are shown in Figure 11f. The β platelets form in the interdendritic liquid before or together with the Al-Si eutectic [10]. This is the same stage in which the measuring arms began to carry load and the tears were initiated. Long platelets subdivide the interdendritic channels and hinder the flow of the residual melt [10]. In an Al-Mg-Si alloy, the amount of plate-like β-$Al_5FeSi$ was even identified as the primary factor controlling hot tearing [13]. Shorter and more compact Fe-rich phases leave more of the channel cross-section open for feeding. This agrees with the behaviour of the Nb 0.15 alloy, in which two arms with visible tears built up a load comparable to that of the intact arms.

**Table 9.** Mean length of the β-$Al_5FeSi$ platelets in the AlSi5Cu2Mg alloy without and with Nb addition, determined on metal-mould samples. Adapt from [22].

| Alloy | Without Nb | Nb 0.10 | Nb 0.15 | Nb 0.20 |
|---|---|---|---|---|
| β-$Al_5FeSi$ length [µm] | 22.6 | 19.1 | 14.9 | 11.6 |

Both changes follow the same trend as reported for Nb-B inoculation, where the size of the β-Fe precipitates decreased together with the α-Al grain size [21]. They are also consistent with reports that Nb-based additions remain effective in Si-rich alloys [19]. This is a key difference from titanium, which in Al-Si alloys partly transforms into Ti-Si-containing phases that are not effective nucleants [15]. In the same AlSi5Cu2Mg alloy, additions of 0.1–0.3 wt.% Ti reduced $HTI_1$ by 14–26% and $HTI_3$ by 7–28% [4]. These alloys remained in the moderate or high susceptibility category. Niobium, added in much smaller measured amounts (0.049–0.076 wt.%), reduced the same indices by 65–91% and moved the alloy to the minimal or low category. This comparison indicates that niobium is a more efficient addition for this alloy than titanium.

At the highest addition, the finer dendrites and shorter Fe-rich phases did not lead to a further improvement. Although this alloy had the smallest SDAS (16.58 µm) and the shortest β-$Al_5FeSi$ platelets (11.6 µm), its HTI values rose again and its anchored arm performed worse than that of the reference alloy. Unlike an excessive Ti addition to the same alloy, where sharp-edged Ti-rich particles were found at the site of tear initiation [4], no coarse Nb-rich particles were observed. The higher Si content of this alloy (6.82 wt.%) would also be expected to improve rather than impair feeding. A possible explanation lies in the permeability of the mushy zone. Although a finer dendritic network provides more channels, each of them is narrower, and in the final stage of solidification the permeability decreases with the square of the dendrite arm spacing [5,29]. As long as the strain is moderate, the larger number of channels prevails, which agrees with the low HTI values of all Nb alloys. Under the severe restraint of the anchored arm, however, the contraction must be compensated by a faster flow of liquid, and the narrow channels of the Nb 0.20 alloy were no longer able to supply it. The free dendrite arms and the microshrinkage at the tear edges (Figure 11) support this explanation and show that the tears in this alloy opened in the presence of interdendritic liquid, when the feeding of the mushy zone failed.

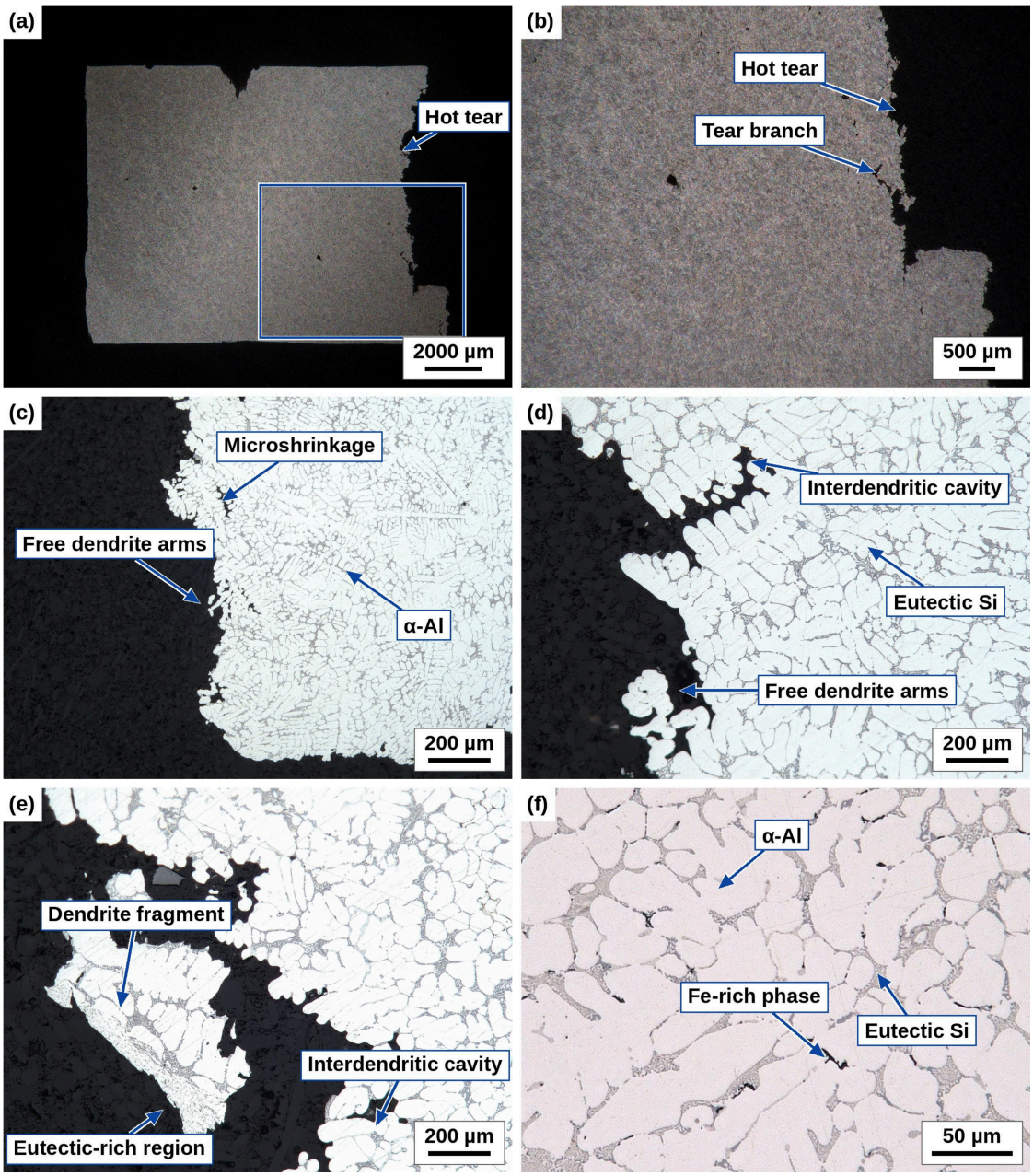



**Figure 11.** Hot tear in the measuring arm of the Nb 0.20 alloy: (**a**) macroscopic cross-section of the arm (the frame marks the area shown in (**b**)); (**b**) detail of the tear edge; (**c**–**e**) tear profiles, etched with 0.5% HF; (**f**) microstructure next to the tear after etching for Fe-rich phases.

## 4. Conclusions

This study investigated the effect of nominal Nb additions of 0.10, 0.15 and 0.20 wt.% (measured 0.049, 0.063 and 0.076 wt.%), introduced through an AlNb10 master alloy, on the hot tearing susceptibility of the AlSi5Cu2Mg alloy. The following conclusions can be drawn:

1. All Nb additions reduced the three hot tearing indices compared with the reference alloy ($HTI_1 = 0.93$, $HTI_2 = 2.35$, $HTI_3 = 1.91$). The lowest values, $HTI_1 = 0.18$, $HTI_2 = 0.60$ and $HTI_3 = 0.17$, were obtained for the nominal 0.15 wt.% addition, which corresponds to minimal to low susceptibility. The differences between the Nb alloys were within the scatter of the results; however, only for this addition did the range of mean ± standard deviation not overlap with that of the reference alloy for any of the three indices.

2. The anchored measuring arm also indicated the nominal 0.15 wt.% addition as the most favourable. It was the only variant in which every arm transferred load. Four of its five arms built up the load continuously to 848–1137 N, compared with 940–1030 N for the three intact arms of the reference alloy.
3. Under the severe restraint of the anchored arm, the Nb 0.10 alloy behaved like the reference alloy. The Nb 0.20 alloy performed worse: two of its arms separated immediately, a third transferred less than 120 N and no arm remained free of tears, although its HTI values remained below those of the reference alloy.
4. Niobium refined the dendritic structure. The SDAS decreased from 25.76 µm for the reference alloy to 20.06, 18.36 and 16.58 µm with increasing Nb addition. Together with the previously reported shortening of the β-$Al_5FeSi$ platelets from 22.6 to 11.6 µm, this facilitates the feeding of the mushy zone under moderate restraint. At the highest addition, the narrower interdendritic channels probably limited the flow of the residual liquid under severe restraint.
5. The hot tears formed in the final stage of solidification, before or at the onset of load build-up, in the presence of residual interdendritic liquid, as indicated by the free dendrite arms and microshrinkage on the tear walls.

Niobium added without boron is thus a promising way to reduce the hot tearing susceptibility of the Ti-restricted AlSi5Cu2Mg alloy, with the most favourable results at the nominal 0.15 wt.% addition. In the longer term, such additions could help to cast cylinder heads of more complex shape with a lower risk of hot tears and to make wider use of recycled material, in which the morphology of the Fe-rich phases plays an important role.

**Author Contributions:** Conceptualization, M.S. and D.B.; methodology, M.S. and M.M.; formal analysis, M.S. and M.M.; investigation, M.S.; writing—original draft preparation, M.S.; writing—review and editing, D.B. and M.M.; visualization, M.S.; supervision, D.B.; funding acquisition, D.B. All authors have read and agreed to the published version of the manuscript.

**Funding:** This research was funded by the Cultural and Educational Grant Agency (KEGA) of the Ministry of Education, Science, Research and Sport of the Slovak Republic, Grant No. 003ŽU-4/2024, and by the Grant System of the University of Žilina (UNIZA), Grant No. 21156. The authors gratefully acknowledge this support.

**Data Availability Statement:** The original contributions presented in this study are included in the article. Further inquiries can be directed to the corresponding author.

**Conflicts of Interest:** The authors declare no conflicts of interest.

## References

1. Zhang, M.; Tian, Y.; Zheng, X.; Zhang, Y.; Chen, L.; Wang, J. Research Progress on Multi-Component Alloying and Heat Treatment of High Strength and Toughness Al–Si–Cu–Mg Cast Aluminum Alloys. *Materials* **2023**, *16*, 1065. [CrossRef] [PubMed]
2. Mohamed, A.M.A.; Samuel, E.; Zedan, Y.; Samuel, A.M.; Doty, H.W.; Samuel, F.H. Intermetallics Formation during Solidification of Al–Si–Cu–Mg Cast Alloys. *Materials* **2022**, *15*, 1335. [CrossRef] [PubMed]
3. Matejka, M.; Bolibruchová, D.; Kantoríková, E. Study of Susceptibility to Tearing of AlSi5Cu2Mg Alloy with Addition of Zr and Ti. *Arch. Foundry Eng.* **2024**, *24*, 107–114. [CrossRef]
4. Matejka, M.; Bolibruchová, D.; Sýkorová, M. Effect of Ti Addition on the Hot-Tearing Susceptibility of the AlSi5Cu2Mg Alloy. *Metals* **2024**, *14*, 703. [CrossRef]
5. Eskin, D.G.; Suyitno; Katgerman, L. Mechanical Properties in the Semi-Solid State and Hot Tearing of Aluminium Alloys. *Prog. Mater. Sci.* **2004**, *49*, 629–711. [CrossRef]
6. Li, S.; Apelian, D. Hot Tearing of Aluminum Alloys: A Critical Literature Review. *Int. J. Met.* **2011**, *5*, 23–40. [CrossRef]
7. Li, Y.; Li, H.; Katgerman, L.; Du, Q.; Zhang, J.; Zhuang, L. Recent Advances in Hot Tearing during Casting of Aluminium Alloys. *Prog. Mater. Sci.* **2021**, *117*, 100741. [CrossRef]
8. Campbell, J. *Complete Casting Handbook: Metal Casting Processes, Metallurgy, Techniques and Design*, 2nd ed.; Butterworth-Heinemann: Oxford, UK, 2015.

9. Taylor, J.A. Iron-Containing Intermetallic Phases in Al-Si Based Casting Alloys. *Procedia Mater. Sci.* **2012**, *1*, 19–33. [CrossRef]
10. Lu, L.; Dahle, A.K. Iron-Rich Intermetallic Phases and Their Role in Casting Defect Formation in Hypoeutectic Al–Si Alloys. *Metall. Mater. Trans. A* **2005**, *36*, 819–835. [CrossRef]
11. Easton, M.; StJohn, D.; Sweet, L. Grain Refinement and Hot Tearing of Aluminium Alloys—How to Optimise and Minimise. *Mater. Sci. Forum* **2009**, *630*, 213–221. [CrossRef]
12. Vicario Gómez, I.; Villanueva Viteri, E.; Montero, J.; Djurdjevic, M.; Huber, G. The Determination of Dendrite Coherency Point Characteristics Using Three New Methods for Aluminum Alloys. *Appl. Sci.* **2018**, *8*, 1236. [CrossRef]
13. Liang, K.Y.; Huang, H.C.; Tseng, C.Y.; Chen, M.C.; Lee, S.L.; Lin, C.C.; Su, T.C. Effects of Fe, Si, Cu, and TiB2 Grain Refiner Amounts on the Hot Tearing Susceptibility of 5083, 6061, and 7075 Aluminum Ingots. *Metals* **2024**, *14*, 15. [CrossRef]
14. Li, P.; Sui, Y.; Jiang, Y.; Yuan, Y.; Yang, H.; Yang, J. Optimizing Hot Tearing Susceptibility of Al-5.5Zn-2.4Mg-1.3Cu Alloys by Grain Refinement, Increasing Mold and Casting Temperature. *Mater. Des.* **2024**, *246*, 113325. [CrossRef]
15. Samuel, E.; Tahiri, H.; Samuel, A.M.; Samuel, F.H. Heterogenous Grain Nucleation in Al-Si Alloys: Types of Nucleant Inoculation. *Metals* **2024**, *14*, 271. [CrossRef]
16. Knipling, K.E.; Dunand, D.C.; Seidman, D.N. Criteria for Developing Castable, Creep-Resistant Aluminum-Based Alloys—A Review. *Z. Met.* **2006**, *97*, 246–265. [CrossRef]
17. Nowak, M.; Bolzoni, L.; Hari Babu, N. Grain Refinement of Al–Si Alloys by Nb–B Inoculation. Part I: Concept Development and Effect on Binary Alloys. *Mater. Des.* **2015**, *66*, 366–375. [CrossRef]
18. Bolzoni, L.; Nowak, M.; Hari Babu, N. Grain Refinement of Al–Si Alloys by Nb–B Inoculation. Part II: Application to Commercial Alloys. *Mater. Des.* **2015**, *66*, 376–383. [CrossRef]
19. Bolzoni, L.; Hari Babu, N. Engineering the Heterogeneous Nuclei in Al-Si Alloys for Solidification Control. *Appl. Mater. Today* **2016**, *5*, 255–259. [CrossRef]
20. Bolzoni, L.; Xia, M.; Hari Babu, N. Formation of Equiaxed Crystal Structures in Directionally Solidified Al-Si Alloys Using Nb-Based Heterogeneous Nuclei. *Sci. Rep.* **2016**, *6*, 39554. [CrossRef] [PubMed]
21. Narducci, C.J.; Brollo, G.L.; de Siqueira, R.H.M.; Antunes, A.S.; Abdalla, A.J. Effect of Nb Addition on the Size and Morphology of the β-Fe Precipitates in Recycled Al-Si Alloys. *Sci. Rep.* **2021**, *11*, 9613. [CrossRef] [PubMed]
22. Sýkorová, M.; Bolibruchová, D.; Matejka, M. Effect of Niobium on the Size and Morphology of Fe-Rich Intermetallic Phases in an AlSi5Cu2Mg Alloy. *Arch. Foundry Eng.* **2026**, *26*, 112–117. [CrossRef]
23. Bolibruchová, D.; Sýkorová, M.; Brůna, M.; Matejka, M.; Širanec, L. Effect of Zr Addition on Selected Properties and Microstructure of Aluminum Alloy AlSi5Cu2Mg. *Int. J. Met.* **2023**, *17*, 2598–2611. [CrossRef]
24. Silva, E.L., Jr.; Kultz Unti, L.F.; Tosetti, J.P.V.; Antunes, A.S.; Zilnyk, K. Grain Refining and Fading Mechanisms in a Eutectic Al-Si Alloy Refined with Al-Nb-B. *J. Alloys Compd.* **2025**, *1042*, 183914. [CrossRef]
25. Wu, Q. Study of Hot Tearing in Cast and Wrought Aluminum Alloys. Master's Thesis, Worcester Polytechnic Institute, Worcester, MA, USA, 2012.
26. Akhyar, H.; Malau, V.; Suyitno; Iswanto, P.T. Hot Tearing Susceptibility of Aluminum Alloys Using CRCM-Horizontal Mold. *Results Phys.* **2017**, *7*, 1030–1039. [CrossRef]
27. Song, J.; Pan, F.; Jiang, B.; Atrens, A.; Zhang, M.-X.; Lu, Y. A Review on Hot Tearing of Magnesium Alloys. *J. Magnes. Alloy.* **2016**, *4*, 151–172. [CrossRef]
28. Easton, M.; StJohn, D. Grain Refinement of Aluminum Alloys: Part I. The Nucleant and Solute Paradigms—A Review of the Literature. *Metall. Mater. Trans. A* **1999**, *30*, 1613–1623. [CrossRef]
29. Rappaz, M.; Drezet, J.-M.; Gremaud, M. A New Hot-Tearing Criterion. *Metall. Mater. Trans. A* **1999**, *30*, 449–455. [CrossRef]


**Disclaimer/Publisher's Note:** The statements, opinions and data contained in all publications are solely those of the individual author(s) and contributor(s) and not of MDPI and/or the editor(s). MDPI and/or the editor(s) disclaim responsibility for any injury to people or property resulting from any ideas, methods, instructions or products referred to in the content.